Small Structures

small structures

www.small-structures.com

RESEARCH ARTICLE OPEN ACCESS

Barium Strontium Titanate Thin Film for Electrically Tunable THz Metasurface

Nour Al Meselmene[1,2] | Piyush Agarwal[1] | Jichao Fu[1,3] | Kandammathe Valiyaveedu Sreekanth[1,3] | Siew Lang Teo[1] | Ai Jia Sim[1] | Karen Lin Ke[1] | Ping Yang[4] | Arash Nemati[1] | Elhadj Dogheche[2] | Jinghua Teng[1,3]

[1]Institute of Materials Research and Engineering, Agency for Science Technology and Research (A*STAR), Singapore, Republic of Singapore | [2]Institut d'Electronique, de Microélectronique et de Nanotechnologie-Site de Valenciennes, IEMN CNRS UMR, Université Polytechnique Hauts-de-France (UPHF), Valenciennes, France | [3]National Semiconductor Translation and Innovation Centre (NSTIC), Singapore, Republic of Singapore | [4]Singapore Synchrotron Light Source (SSLS), National University of Singapore (NUS), Singapore, Republic of Singapore

Correspondence: Arash Nemati (arash.nemati80@gc.cuny.edu) | Elhadj Dogheche (elhadj.dogheche@uphf.fr) | Jinghua Teng (jh-teng@imre.a-star.edu.sg)

Received: 24 May 2025 | **Revised:** 20 October 2025 | **Accepted:** 28 October 2025

Keywords: barium strontium titanate (BST) | electrically tunable metasurface | ferroelectrics | interdigitated electrodes (IDE) | metasurface | terahertz (THz)

ABSTRACT

Barium strontium titanate (BST) thin films are distinguished for their ferroelectric behavior which makes them highly promising for optical and microwave applications, but there is a lack of studies in the important terahertz (THz) frequency range. In this work, we report the deposition of high-quality BST films by physical vapor deposition at high temperatures and its application in tunable THz metadevices. The $Ba_{0.6}Sr_{0.4}TiO_3$ film exhibits a full width at half maximum of 0.57° in high-resolution X-ray diffraction (HR-XRD) spectroscopy, a real dielectric constant of 140 at 0.2 THz. By integrating interdigitated electrodes (IDEs) of varying periodicities, we systematically investigated their impact and identified a 100 µm electrode separation as the optimal electrode separation for maximizing THz response modulation. A metasurface using $Ba_{0.6}Sr_{0.4}TiO_3$ thin film as the active material working in reflection mode has been designed using finite-difference time-domain (FDTD) simulation, and the fabricated metadevice experimentally demonstrated a remarkable resonance shifts of up to 5.5 GHz under applied voltage. These findings underscore the potential of BST for reconfigurable intelligent metasurfaces and future electrically tunable THz device applications.

1 | Introduction

Terahertz (THz) electromagnetic radiation, spanning the frequency range between the microwave and optical domains, has attracted growing attention due to its potential in a wide array of applications, including high-speed communication [1], imaging [2], and sensing [3]. THz waves have the potential to investigate subsurface layers, resonate with molecular vibrations, and support ultrahigh data rates. Advancing THz technologies requires the development of compact, efficient, and tunable components, particularly solid-state devices capable of active control. Different materials and different control methods (magnetic, optical, electrical, thermal) have been investigated to achieve tunable THz response [4–8].

Metamaterials and metasurfaces, engineered to manipulate electromagnetic waves through subwavelength structures, are promising candidates for THz applications owing to their versatile and designable properties [7–10]. A critical challenge, however, lies in integrating suitable active materials that enable dynamic tunability. Several approaches have been explored, including phase-change materials (PCMs) such as vanadium dioxide (VO_2) [11, 12] and germanium-antimony-tellurium (GST) [13], which offer large refractive index modulation but suffer from thermal instability and high-power consumption. Liquid crystals enable voltage-controlled tuning with good uniformity but are limited by slow response times [14]. MEMS-based THz modulators provide precise actuation and CMOS compatibility yet introduce fabrication complexity and mechanical reliability concerns [15].

Two-dimensional (2D) materials, with their high carrier mobility and fast response, show promise but face scalability and integration barriers [16, 17].

Ferroelectric materials, like barium strontium titanate (BST), have attracted significant interest due to their large tunability, nonlinear properties, and compatibility with voltage-controlled devices in optical [18, 19] and microwave regions [20, 21] Extending these properties into the THz region could advance device performance and functionality especially at the frequency range between one and several hundred GHz for 6G applications as it offers extensive bandwidth, lower latency, and enhanced data transfer rates [1]. Tunable metadevices in the THz range using BST as the active material have been reported based on temperature tuning [22] and an electron transport mechanism in which the modulation relies on carrier transport at a conductive interface in sputtered BST films grown on silicon [23]. Electrical tuning of the dielectric properties of BST deposited via the sputtering method for THz device application is much more desirable and effective for real-world applications, yet it has not been reported before.

In this work, we investigate the dielectric property and the electrical tunability of BST thin films in two different compositions, $Ba_{0.6}Sr_{0.4}TiO_3$ and $Ba_{0.5}Sr_{0.5}TiO_3$, deposited by a physical vapor deposition system at high temperatures. Using THz time-domain spectroscopy (THz-TDS), we measure a high dielectric constant of 140 at 0.2 THz in $Ba_{0.6}Sr_{0.4}TiO_3$. We design and fabricate an electrically tunable THz metasurface in reflection mode based on interdigitated electrodes (IDEs) and inductor–capacitor–resistor (LCR) resonant structures on $Ba_{0.6}Sr_{0.4}TiO_3$. The metadevice demonstrates a resonance frequency shift of up to 5.5 GHz under applied voltage, highlighting the promise of BST for compact, tunable THz systems.

2 | BST Deposition and Characterization

BST thin films with two compositions, $Ba_{0.5}Sr_{0.5}TiO_3$ (BST50) and $Ba_{0.6}Sr_{0.4}TiO_3$ (BST60), were deposited to a thickness of 450 nm on *a*-axis-oriented magnesium oxide (MgO) substrates using unbalanced magnetron sputtering. The substrate temperature was maintained at 900°C during deposition, with pure argon as the process gas at a chamber pressure of 8 mTorr. MgO was chosen due to its low refractive index and minimal loss in the THz frequency range (Supporting Information S1), making it an excellent platform for terahertz device applications.

The deposited BST films showed smooth and uniform surfaces free of cracks, as confirmed by the atomic force microscopy (AFM, Bruker, Dimension ICON) (Figure S2, Supporting Information). Figure 1a is the photo of the BST on the MgO sample (2 cm × 2 cm) put on the A*STAR logo shows the high transparency of our BST films.

Structural characterization of the films was conducted using high-resolution X-ray diffraction (HRXRD, Huber, 90000–0216/0 system) to evaluate the crystal quality and transmission electron microscopy (TEM, FEI, Titan) to examine microstructural features. Both BST50 and BST60 exhibited a single-crystal structure oriented along the (00l) direction, as illustrated in Figure 1b. BST60 demonstrated better crystal quality than BST50, as indicated by its smaller full width at half maximum (FWHM) value of 0.57° versus 0.82° for BST50 (Figure 1c). In addition, higher tetragonality and relaxation were observed in BST60 based on reciprocal space mapping measurements of spreading out the BST along (002) (Figure 1d,e) and (−204) (Figure 1f,g). Figure 1h,i represent the TEM images where the BST layers are visible (layer by layer), with a well-defined grain structure, indicating that the growth is highly oriented. Fast Fourier transform (FFT) analysis indicates high crystallinity and well-ordered structure as shown by the sharp lattice diffraction spots.

THz characterization of the BST film is performed using THz-TDS in transmission mode to provide insights into the dielectric response and in reflection mode to evaluate the tunability and resonance shift of the active THz metasurface under an applied electric field. The THz-TDS measurements were conducted up to 1 THz [24], in which the BST film covered only half of the MgO substrate with the other half of the bare MgO substrate used as a reference. Figure 1j shows the evolution of the real dielectric constant and the tangent loss (tan δ) with frequency for both BST50 and BST60. At 0.25 THz, the real dielectric constant (ε) of BST60 was 125, higher than that of BST50 of value 100, which aligns well with values reported for the same composition [25]. The soft mode for BST60 was observed at around 0.3 THz and the corresponding ionic polarization relaxation was found to decrease the dielectric loss making it suitable for applications at lower terahertz frequencies [26]. Both compositions showed a monotonic decrease in the dielectric constant as frequency increased, without exhibiting dielectric domain behavior. On the other hand, the tangent loss (tan δ) increased monotonically with frequency. It can be seen from Figure 1j that BST60 possesses a higher dielectric constant and lower tangent loss than BST50. The improved performance of BST60 can be attributed to its higher Ba content, which enhances ionic polarizability and introduces beneficial lattice strain. Combined with better crystalline quality (as indicated by HR-XRD), these factors contribute to both higher dielectric constants and reduced energy dissipation. Notably, the BST60 film reported here outperforms commonly studied materials such as lithium niobate in terms of dielectric response in the THz regime [27].

3 | BST for Tunable Metasurface

3.1 | Tunability of BST Film at THz Range

To evaluate the dielectric tunability of the BST films under electrical bias, interdigital electrodes (IDEs) were fabricated on both BST50 and BST60 films. Each IDE pattern had a finger width of 10 μm and a gap of 100 μm (Figure 2a). The IDEs were patterned by photolithography and standard lift-off process, where Cr/Au electrical contact was deposited by e-beam evaporation. A scanning electron microscope (SEM) image of the fabricated IDEs is shown in Figure 2b, illustrating well-defined and uniform structures.

Dielectric tunability was characterized using THz-TDS in transmission mode under varying electric fields. Upon applying a DC electric field, the Ti^{4+} cations at the B-site in the perovskite

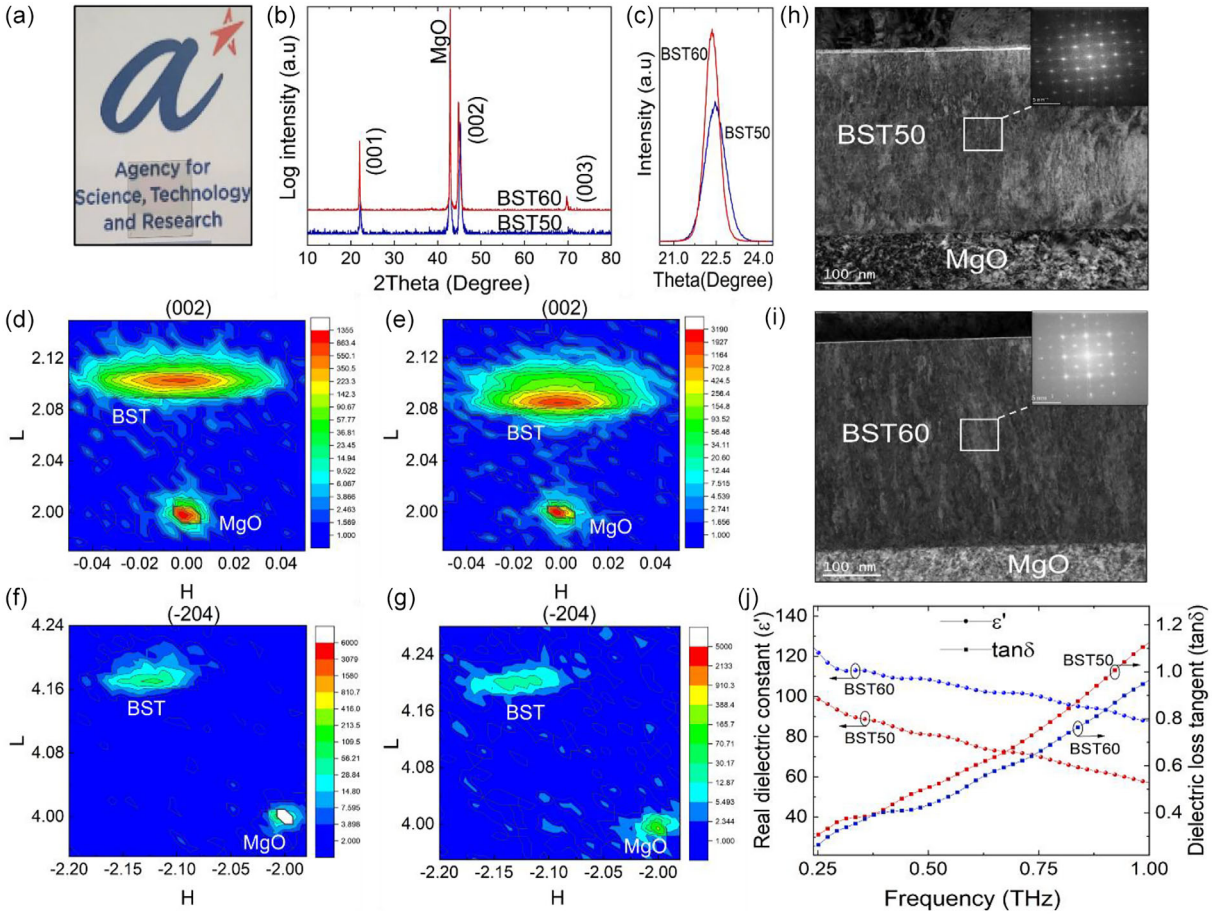

FIGURE 1 | Structural and dielectric constant characterization of the deposited BST films on MgO substrate. (a) Photo of the obtained BST film on top of the A*STAR logo. (b) HR-XRD 2θ-ω scan for both BST50 and BST60 films. (c) The comparison of the FWHM of the (002) peak for BST50 and BST60 films. (d–g) RSM plots along the (002) and (−204) directions for BST50 and BST60 films. (h,i) TEM images of the BST layers, along with their FFT images. (j) Comparison of the real part of the dielectric constant (solid circles) and tangent loss (solid squares) for BST50 (red) and BST60 (blue) films measured at room temperature.

structure are displaced relative to the negatively charged oxygen octahedra, forming electric dipoles [28]. This lattice polarization alters the interaction between the THz field and the material, reducing the dielectric constant as the polarization response becomes saturated.

Figure 2c compares the tunability of BST50 and BST60 under an applied electric field of 5 V/μm. BST60 exhibited a significantly higher tunability, which is attributed to its superior crystal quality and enhanced tetragonal phase. These characteristics promote more efficient field-induced dipole reorientation and polarization modulation. The additional fluctuations observed in its tunability spectra likely originate from local polarization inhomogeneities and bias-induced soft-mode dynamics. The higher dielectric constant and lower energy loss of BST60 also contribute to its improved performance. Interestingly, this trend contrasts with previous observations in the microwave regime, where BST50 generally outperforms other compositions [20].

The effect of IDE gap size on the tunability in the THz frequency range was further investigated using BST60. Three different gap sizes: 20, 100, and 200 μm, were fabricated on BST60 films deposited under identical conditions. The dielectric tunability results were measured at an applied electric field of 2.5 V/μm and illustrated in Figure 2d. The diagrams indicate that the 100 μm gap size resulted in the highest dielectric tunability at lower THz frequencies, followed by the 200 μm gap, while the 20 μm gap size had the lowest tunability. This observation could be attributed to the electric field distribution and interaction volume within the BST film, where the dielectric tunability percentage depends on two factors: the applied DC field (changes the dielectric constant), and the THz electric field which probes these changes. To support the experimental findings, FDTD simulations were performed. The THz transmission spectra were simulated for three different gap sizes using the experimentally extracted dielectric constants. The results, presented in the (Figure S3, Supporting Information), confirm that a pronounced resonance dip in the transmission spectrum appears only for the 100 μm gap, validating the observed superior tunability. The enhanced resonance originates from the localization of the THz wave at 100 mm gap pattern, where overlap between the modulated dielectric region and the incident field is maximized. This creates a more efficient tuning environment, amplifying the BST film's response under bias. A more detailed analysis of the THz electric field distribution and transmission behavior under varying voltages for the 100 μm gap is provided in Figures S3 and S4, Supporting Information. These findings guide the optimized design of the electrically tunable THz metasurface based on BST presented in the following section.

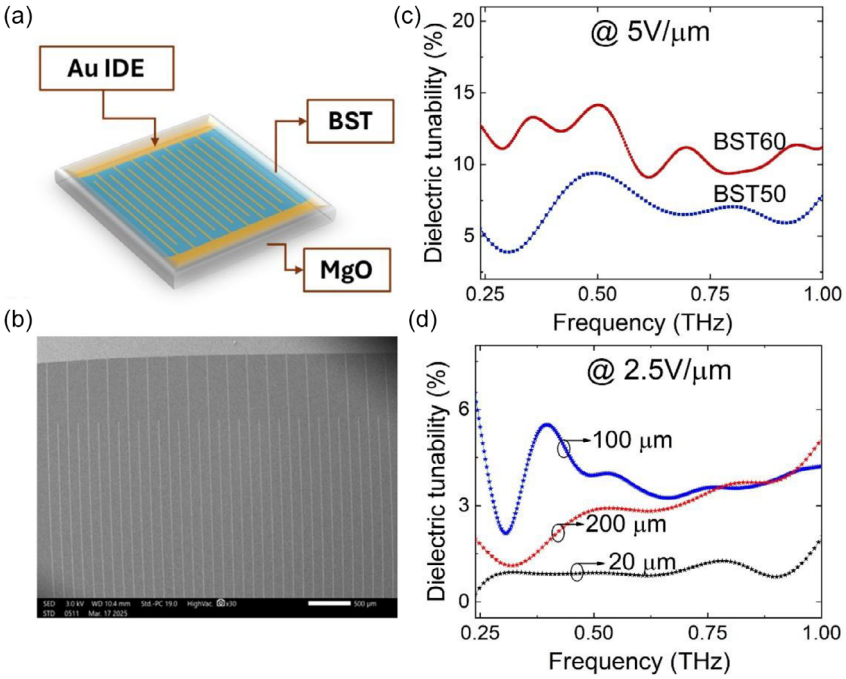

FIGURE 2 | Dielectric tunability of BST films under applied electric field using IDE structures. (a) 3D Schematic of the IDE configuration patterned on the BST films. (b) SEM image of fabricated IDEs with a 100 μm gap. (c) Measured tunability of BST50 and BST60 films at 5 V/μm electric field. (d) Comparison of dielectric tunability in BST60 for IDE gaps of 20 μm (black), 100 μm (blue), and 200 μm (red).

3.2 | Electrically Tunable THz Metasurface

An electrically tunable terahertz (THz) metasurface operating in reflection mode was designed using the BST60 thin film as the active material. The metasurface unit cell, shown schematically in Figure 3a, consists of an inductor-capacitor-resistor (LCR) antenna structure placed atop the BST film. The optimized geometrical parameters of the unit cell are: Px = 100 μm, Py = 180 μm, A = 75 μm, W = 8 μm, G = 12 μm, and D = 12 μm.

Figure 3b illustrates the overall metasurface layout, consisting of an array of LCR unit cells integrated with IDEs to facilitate

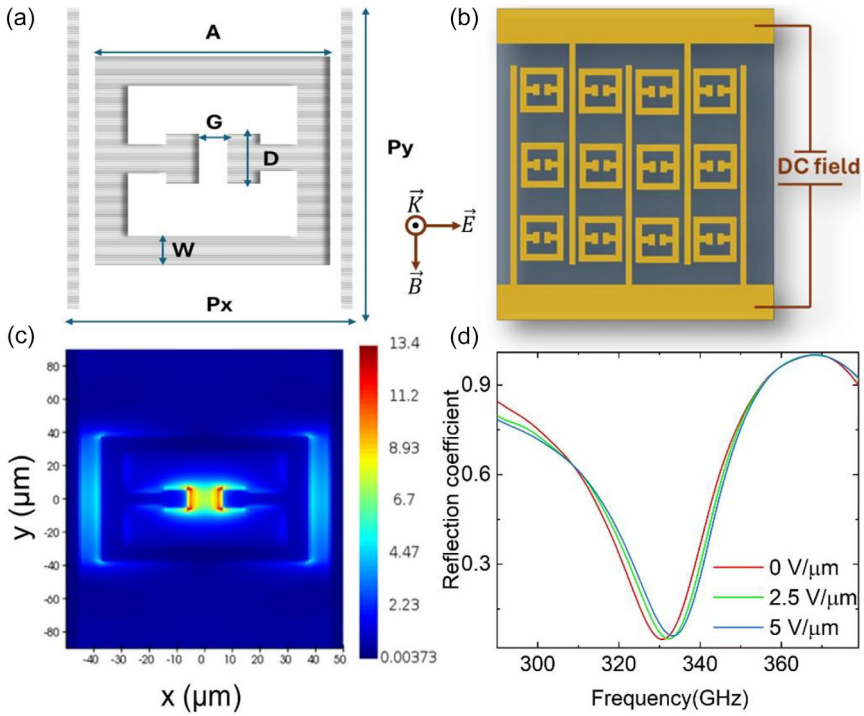

FIGURE 3 | Electrically tunable metasurface on BST. (a) Schematic of LCR unit cell geometry. (b) Layout of the metasurface array with IDE structures and external voltage pads. (c) Simulated electric field distribution showing field localization at the LCR gap. (d) Simulated reflection spectra for applied fields ranging from 0 to 5 V/μm.

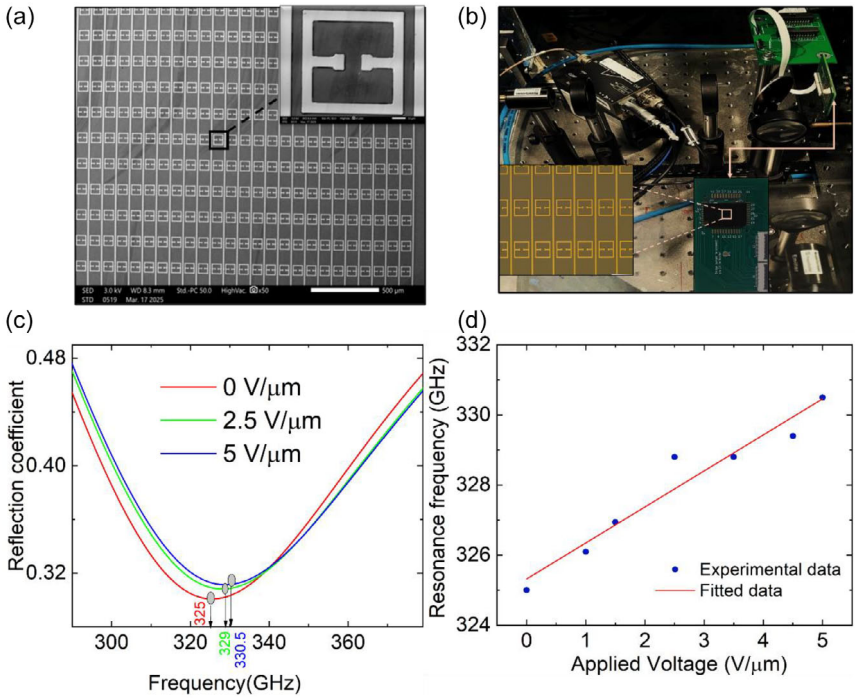

FIGURE 4 | Experimental characterization of the THz metasurface. (a) SEM image of the fabricated metasurface with zoom-in of the unit cell shown in the inset. (b) Experimental setup for testing the tunable metasurface in reflection mode, with the inset showing the fabricated sample mounted on a PCB. (c) Measured reflection spectra at applied fields of 0, 2.5, and 5 V/μm. (d) Extracted resonance frequency shift versus applied electric field.

external voltage application. The IDE fingers and antenna lines were fabricated using 200-nm-thick Au with 10 μm width. The IDE structure allows lateral electric fields to be applied across the BST layer, thereby modulating its dielectric properties.

The local electromagnetic fields of the LCRs overlap with the BST60 thin film, leading to the creation of strong coupling between the fields and the material. The electric field distribution of the THz wave has been simulated and is shown in Figure 3c. The resonance of the THz wave is determined by the parameters of the LCRs, especially sensitive to the Gap G. The response of the metasurface to the THz wave is highly sensitive to the environment change in the LCRs. Any modification in the dielectric properties of the BST60 thin film will directly affect the resonance behavior of the metasurface by inducing a shift in the resonance frequency. By applying a voltage to the IDE pads, the dielectric constant of the BST thin film will be tuned, which, in turn, will change the metasurface resonance. Figure 3d shows the simulated spectral response of the THz metasurface to the applied external voltage (Figure S5, Supporting Information). The resonance frequency shifts from 0.330 to 0.335 THz when the dielectric constant of the BST60 thin film is reduced by 11%, corresponding to an electric field increase from 0 to 5 V/μm.

Figure 4a is the SEM image of the fabricated THz metasurface and zoom-in image of the unit cell together with IDE in the inset, showing well-defined structures without defects. The fabricated metasurface was mounted on a printed circuit board (PCB) and tested in reflection mode, as illustrated in Figure 4b. The measured reflection spectra of the metasurface at different electric fields are shown in Figure 4c and matched well with the simulation results. We observed resonance peaks with central frequencies near 0.325, 0.329, and 0.3305 THz for the electric fields of 0, 2.5, and 5 V/μm, respectively. The resonant frequency of the metasurface increases with increasing electric field applied between the IDE fingers. The electric field-induced resonance tuning has a close to linear relationship between the resonant frequency and the applied external voltage, as depicted in Figure 4d. The strength of the electric field in the gap region makes the LCR resonance frequency sensitive to changes in dielectric constant of the BST film, which directly affects the effective capacitance C. The resonant frequency shifts to high frequency as the dielectric constant of the BST film decreases with increasing electric field.

The reflection spectra in the experiments exhibit a broader and more diffuse peak compared to the simulated data at the resonance frequencies. This suppression of the resonance peak is likely caused by background noise originating from the detection and small differences between the designed and fabricated devices due to fabrication deviation. Regardless of these discrepancies, the results confirm the effective electrical field-induced tunability of the metasurface in the THz frequency range, with the linear shift in resonance frequency with applied voltage. The results highlight the ability and potentials of using BST as the active material for dynamic THz tuning and control.

4 | Conclusion

Highly epitaxial BST thin films with two compositions, $Ba_{0.5}Sr_{0.5}TiO_3$ (BST50) and $Ba_{0.6}Sr_{0.4}TiO_3$ (BST60), were successfully deposited on MgO substrates and characterized for THz applications. BST60 exhibited superior dielectric performance and stronger electrical tunability compared to BST50, in contrast

to trends typically observed in the microwave regime. IDE structures were used to apply lateral electric fields, with a 100 μm gap identified as optimal, validated through both experiments and simulations, for achieving maximum dielectric tunability at lower THz frequencies. A reflection-mode THz metasurface incorporating LCR unit cells on a 458-nm-thick BST60 film demonstrated a resonance frequency shift of up to 5.5 GHz under a 5 V/μm electric field. These findings establish BST thin films as a promising platform for developing compact, electrically reconfigurable THz photonic devices.

Author Contributions

Jinghua Teng: conceptualization (lead); formal analysis (equal); funding acquisition (lead); investigation (supporting); methodology (equal); project administration (lead); resources (lead); supervision (equal); writing – review and editing (lead). **Nour Al Meselmene**: data curation (lead); formal analysis (lead); investigation (lead); writing – original draft (lead). **Piyush Agarwal**: data curation (lead); formal analysis (lead); writing – review and editing (supporting). **Jichao Fu**: data curation (supporting); formal analysis (supporting); investigation (supporting). **Kandammathe Valiyaveedu Sreekanth**: data curation (supporting); investigation (supporting); writing – review and editing (supporting). **Siew Lang Teo**: investigation (supporting). **Ai Jia Sim**: investigation (supporting). **Karen Lin Ke**: investigation (supporting); supervision (supporting). **Ping Yang**: investigation (supporting); writing – review and editing (supporting). **Arash Nemati**: conceptualization (supporting); formal analysis (supporting); methodology (supporting); supervision (supporting); writing – review and editing (supporting). **Elhadj Dogheche**: conceptualization (supporting); funding acquisition (supporting); resources (supporting); supervision (supporting); validation (supporting); writing – review and editing (supporting).

Acknowledgments

The work was financially supported by the Agency for Science, Technology and Research (A*STAR) under MTC Programmatic Grant (M22L1b0110), the National Research Foundation, Singapore under NRF-CRP (NRF-CRP26-2021-0004), and the National Semiconductor Translation and Innovation Centre (NSTIC) and Université Polytechnique Hauts de France under Program Grant (AAP 2023-1).

Funding

Agency for Science, Technology and Research (A*STAR) (M22L1b0110); National Research Foundation, Singapore (NRF-CRP26-2021-0004); National Semiconductor Translation and Innovation Centre (NSTIC); Université Polytechnique Hauts de France (AAP 2023-1).

Conflicts of Interest

The authors declare no conflicts of interest.

Data Availability Statement

The data that support the findings of this study are available from the corresponding author upon reasonable request.

References

1. T. S. Rappaport, Y. Xing, O. Kanhere, et al., "Wireless Communications and Applications above 100 GHz: Opportunities and Challenges for 6G and beyond," *IEEE Access* 7 (2019): 78729–78757.

2. G. Valušis, A. Lisauskas, H. Yuan, W. Knap, and H. G. Roskos, "Roadmap of Terahertz Imaging 2021," *Sensors* 21 (2021): 4092.

3. S. Shen, X. Liu, Y. Shen, et al., "Recent Advances in the Development of Materials for Terahertz Metamaterial Sensing," *Advanced Optical Materials* 10 (2022): 2101008.

4. Z. Zhou, L. Shen, X. Xing, et al., "Observation of Tunable Terahertz Optical Response in Nanoscale Lithium Ferrite Driven by Magnetic Field and Laser," *Journal of Materiomics* 11, no. 6 (2025): 101068.

5. Z. Zhou, L. Shen, X. Xing, et al., "Tunable THz Response in Cobalt Ferrite via Magnetic Field Modulation," *Applied Physics Letters* 127, no. 3 (2025): 032403.

6. H. Zeng, S. Gong, L. Wang, et al., "A Review of Terahertz Phase Modulation from Free Space to Guided Wave Integrated Devices," *Nanophotonics* 11, no. 3 (2021): 415–437.

7. J. Li, J. Chen, D. Yan, et al., "A Review: Active Tunable Terahertz Metamaterials," *Advanced Photonics Research* 5 (2024): 2300351.

8. A. Nemati, Q. Wang, M. Hong, and J. H. Teng, "Tunable and Reconfigurable Metasurfaces and Metadevices," *Opto-Electronic Advances* 1 (2018): 180009.

9. L. Ding, X. Wang, N. S. S. Ang, C. Lu, V. Suresh, and J. H. Teng, "Ultra-Thin Film Broadband Terahertz Antireflection Coating Based on Impedance Matching Method," *IEEE Journal of Selected Topics in Quantum Electronics* 23 (2017): 8500508.

10. W. M. Zhu, A. Q. Liu, T. Bourouina, et al., "Microelectromechanical Maltese-Cross Metamaterial with Tunable Terahertz Anisotropy," *Nature Communications* 3 (2012): 1274.

11. C. Zheng, R. E. Simpson, K. Tang, et al., "Enabling Active Nanotechnologies by Phase Transition: From Electronics, Photonics to Thermotics," *Chemical Reviews* 122 (2022): 15450–15500.

12. M. Jiang, F. Hu, L. Zhang, et al., "Electrically Triggered VO_2 Reconfigurable Metasurface for Amplitude and Phase Modulation of Terahertz Wave," *Journal of Lightwave Technology* 39 (2021): 3488–3494.

13. L. Guo, X. Ma, Z. Chang, C. Xu, J. Liao, and R. Zhang, "Tunable A Temperature-Dependent GST-Based Metamaterial Absorber for Switching and Sensing Applications," *Journal of Materials Research and Technology* 14 (2021): 772–779.

14. L. Wang, Y. Wang, G. Zong, W. Hu, and Y. Lu, "Liquid Crystal Based Tunable Terahertz Metadevices," *Journal of Materiomics* 11 (2025): 100888.

15. P. Pitchappa, C. P. Ho, L. Cong, R. Singh, N. Singh, and C. Lee, "Reconfigurable Digital Metamaterial for Dynamic Switching of Terahertz Anisotropy," *Advanced Optical Materials* 4 (2015): 391–398.

16. Z. Shi, H. Zhang, K. Khan, et al., "Two-Dimensional Materials Toward Terahertz Optoelectronic Device Applications," *Journal of Photochemistry and Photobiology C: Photochemistry Reviews* 51 (2022): 100473.

17. Z. Wang, K. V. Sreekanth, M. Zhao, J. Nong, Y. Liu, and J. Teng, "Two-Dimensional Materials for Tunable and Non-Linear Metaoptics," *Advanced Photonics* 6 (2024): 034001.

18. K. Takeda, T. Muraishi, T. Hoshina, H. Takeda, and T. Tsurumi, "Dielectric Tunability and Electro-Optic Effect of $Ba_{0.5}Sr_{0.5}TiO_3$ Thin Films," *Journal of Applied Physics* 107 (2010): 074105.

19. K. Brekhov and S. Lavrov, "Electro-Optic Properties of $Ba_{0.8}Sr_{0.2}TiO_3$ Thin Film," *Ceramics International* 47 (2020): 3122–3126.

20. G. Vélu, G. Houzet, L. Burgnies, et al., "Electrical Characterizations of Paraelectric BST Thin Films up to 1 THz: Realization of Microwave Phaseshifters," *Ferroelectrics* 353 (2007): 29–37.

21. J. P. Goud, A. Kumar, K. Sandeep, S. Ramakanth, P. Ghoshal, and K. C. J. Raju, "Tunable Microwave Device Fabrication on Low-Temperature Crystallized $Ba_{0.5}Sr_{0.5}TiO_3$ Thin Films by an Alternating Deposition and Laser Annealing Process," *Advanced Electronic Materials* 7 (2021): 2000905.

22. B. Dong, H. Ma, J. Wang, et al., "A Thermally Tunable THz Metamaterial Frequency-Selective Surface Based on Barium Strontium

Titanate Thin Film," *Journal of Physics D: Applied Physics* 52 (2018): 045301.

23. L. Wu, T. Du, N. Xu, et al., "A New $Ba_{0.6}Sr_{0.4}TiO_3$-Silicon Hybrid Metamaterial Device in Terahertz Regime," *Small* 12 (2016): 2610–2615.

24. A. Gauthier-Brun, J. H. Teng, E. Dogheche, et al., "Properties $In_xGa_{1-x}N$ Film in THz Range," *Applied Physics Letters* 100 (2012): 071913.

25. L. Nedelcu, G. Annino, C. Chirila, L. Trupina, A. C. Galca, and M. G. Banciu, "Investigation of $Ba_{0.6}Sr_{0.4}TiO_3$ Thick Films by Means of a Novel THz-TDS Approach," *Applied Surface Science* 506 (2020): 144807.

26. M. Dutta, X. G. Peralta, A. Bhalla, and R. Guo, "Current Status of Oxide Dielectric Materials for Terahertz Applications–an Overview," *Integrated Ferroelectrics* 166 (2015): 108–139.

27. M. Dutta, C. Ellis, X. G. Peralta, A. Bhalla, and R. Guo, "Terahertz Electrical and Optical Properties of $LiNbO_3$ Single Crystal Thin Films," *Proceedings of SPIE* 9586 (2015): 958608.

28. S. Gevorgian, *Ferroelectrics in Microwave Devices*, *Circuits and Systems: Physics*, *Modeling*, *Fabrication and Measurements* (Springer Science & Business Media, 2009).

Supporting Information

Additional supporting information can be found online in the Supporting Information section. **Supporting Fig. S1:** Refractive index (n) and imaginary part (k) of the MgO substrate measured using THz-TDS. **Supporting Fig. S2:** AFM images of BST thin films: (a) BST60 and (b) BST50. **Supporting Fig. S3:** FDTD-simulated transmission spectra illustrating gap-size-dependent resonance behavior. Electric field distribution of the IDE patterns simulated using FDTD software for a gap size of: (a) 20 μm, (b) 100 μm, and (c) 200 μm. **Supporting Fig. S4:** Simulated transmission amplitudes of the IDE patterns with a gap size value of 100 obtained at 0 V/μm (a) and 2.5 V/μm (b). **Supporting Fig. S5:** Real dielectric constant of the BST60 thin film under different applied voltages from 100 V (purple) to 500 V (green). **Supporting Table S1:** Lattice parameter values for both BST(60) and BST(50) thin films grown on MgO substrate.